

# Fracture Morphology and Local Deformation Characteristics in the Metallic Glass Matrix Composite Under Tension



Y.S. WANG, X.H. SUN, G.J. HAO, Z.X. GUO, Y. ZHANG, J.P. LIN, M.L. SUI,  
and J.W. QIAO

Fracture and deformation characteristics of the Ti-based metallic glass matrix composite have been studied by the tensile test and the *in situ* TEM tension test. Typically, the composite exhibits the high strength and considerable plasticity. Microscopically, it was found that shear deformation zone formed at the crack tip in glass phase, which can bring about quick propagation of shear bands. However, the plastic deformation zone nearby the crack tip in dendrites will postpone or retard the crack extension by dislocations. The attributions of micro-deformations to mechanical properties of composites were discussed.

DOI: 10.1007/s11661-015-3254-0

© The Minerals, Metals & Materials Society and ASM International 2015

## I. INTRODUCTION

**BULK** metallic glasses (BMGs) have attracted intense attentions for the incomparable mechanical properties, *e.g.*, excellent elastic limits, high strengths, and high hardness.<sup>[1–5]</sup> However, due to the unlimited propagation of highly local shear bands, BMGs always display limited plastic deformation in compression and nearly zero plasticity in tension, seriously retarding their engineering applications. To circumvent this disadvantage, metallic glass matrix (MGM) composites containing *ex situ* or *in situ* phase were designed with improved toughness and the considerable tensile plasticity at room temperature. In these alloys, MGM composites containing *in situ* ductile dendritic crystalline phases have gained widespread achievements for sharing the large plastic deformation of dendrites and high strength of the glass phase,<sup>[5–11]</sup> *e.g.*, Ti-,<sup>[2,6]</sup> Zr-,<sup>[3,5,7,8]</sup> Cu-based,<sup>[11]</sup> and Mg-<sup>[10]</sup> MGM composites.

Up to now, researches including the microstructure, mechanical properties, as well as deformation mechanisms of MGM composites have been carried out extensively. It is found that mechanical properties rely on the microstructures,<sup>[12–16]</sup> *e.g.*, dendrite size, volume fraction, spacing, morphology, *etc.* In terms of the micro-mechanisms, many results have been reported

experimentally and theoretically. The plastic deformation occurred first within  $\beta$ -crystal by formation of slip bands.<sup>[3,4,7,14]</sup> The multiplication of slip bands and shear bands is favorable to the macro-plasticity, but the cracks would be initiated at those deepened deformation bands as the deformation proceeds, leading to the final failure.<sup>[7,14]</sup> The fragmentation of the  $\beta$ -crystal phase rather than crystallization within the glass matrix contributes to the high-tensile ductility.<sup>[9]</sup> A tensile deformation model on the basis of elastic-plastic-damage process was proposed according to the work-hardening behavior of dendrites and softening of the glass matrix.<sup>[10]</sup> The tensile necking behavior occurred in  $\beta$ -crystal for the intrinsic low work-hardening rate of the  $\beta$ -crystal under the tensile loading.<sup>[12,13]</sup> Based on the large scale atomistic simulations, plastic shearing events were confined in local glass matrix.<sup>[15]</sup> Moreover, the interaction between the two phases refers to the lattice sliding and the local shear transaction zone.<sup>[15,16]</sup> The 45 deg dendritic inclusions worked better in improving the ductility of MGM composites than that of the 90 deg case.<sup>[17]</sup> However, despite the aforementioned intense understanding of the MGM composites, the direct experimental findings about the localization deformation and micro-damage behavior remain few reports.

On the other hand, the macroscopic fractography cannot reflect the microscopic deformation of the material, which hampers a direct investigation of micro-deformations. The *in situ* tensile test under transmission electron microscopy (TEM) as a powerful tool to directly observe the prohibition, extension, deflection, and multiplication of shear bands as well as the micro-cracks has attracted more and more attentions.<sup>[18–21]</sup> However, few reports refer to study the local deformation and evolution characteristics on MGM composites by *in situ* TEM tensile pattern.<sup>[22,23]</sup> In this paper, fracture morphology and detailed observations of the propagation as well as evolution of shear bands in

Y.S. WANG and J.W. QIAO, Researchers, and X.H. SUN, Student, are with the Laboratory of Applied Physics and Mechanics of Advanced Materials, College of Materials Science and Engineering, Taiyuan University of Technology, Taiyuan 030024, P.R. China. Contact e-mail: wysdoc@hotmail.com G.J. HAO, Y. ZHANG, and J.P. LIN, Researchers, are with the State Key Laboratory for Advanced Metals and Materials, University of Science and Technology Beijing, Beijing 100083, P.R. China. Z.X. GUO, Student, and M.L. SUI, Researcher, are with the Institute of Microstructure and Property of Advanced Materials, Beijing University of Technology, Beijing 100124, P.R. China.

Manuscript submitted May 12, 2015.

Article published online November 25, 2015

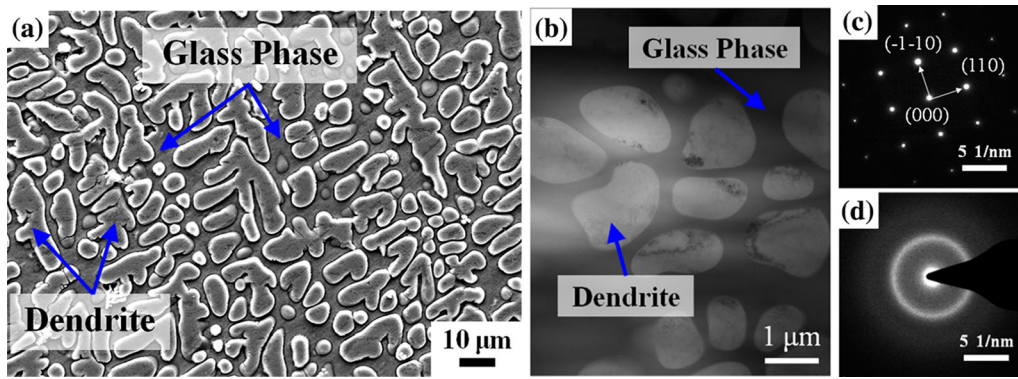


Fig. 1—Representative microstructure a Ti-based MGM composite under SEM (a) and TEM pattern (b). The SAED patterns of the dendrite phase (c), and the amorphous phase (d).

the MGM composite are investigated by the tensile loading and *in situ* transmission electron microscopy tensile test.

## II. EXPERIMENTAL

Ingots the nominal composition of  $\text{Ti}_{47}\text{Zr}_{19}\text{Be}_{15}\text{V}_{12}\text{Cu}_7$  (atomic percentage) were prepared by arc-melting a mixture high-purity elements (purity >99.9 wt pct) under the Ti-gettered argon atmosphere. Rod-like MGM composites with a diameter of 7 mm and a length of 100 mm were fabricated by the Bridgman solidification apparatus.<sup>[24]</sup> Scanning electron microscopy (SEM) was used to observe the microstructure of samples and the fracture features. The dog-bone-like uniaxial tensile specimens with the gage dimensions of 10 mm × 2 mm × 1 mm (length × width × thickness) were cut by the electric spark method. After grinding and polishing specimens using a 1.0 μm diamond paste, four specimens were subjected to tensile tests by an Instron 5969 testing machine at a nominal strain rate of  $10^{-4} \text{ s}^{-1}$ .

Foils for the *in situ* TEM tensile test were thinned by the ion milling using a combination of liquid nitrogen temperature to produce a central hole. A Gatan model 654 single-tilt straining holder TEM operating at 300 kV was employed for *in situ* TEM observations. During loading, the experiment was interrupted several times by manual operating to observe the different deformation characteristics.<sup>[23,25]</sup>

## III. RESULTS

### A. Microstructure

Figure 1 shows the microstructure of the Ti-based MGM composite. The dendrite phase with volume fraction of 41 pct is homogeneously embedded in the amorphous phase. Figure 1(b) displays the typical bright-field TEM image of a composite sample. The body-centered cubic structure dendrite with lattice parameter of 0.3201 nm and the glass phase with homogeneous maze were identified by the selected area electron diffraction pattern as shown in Figures 1(c) and (d).

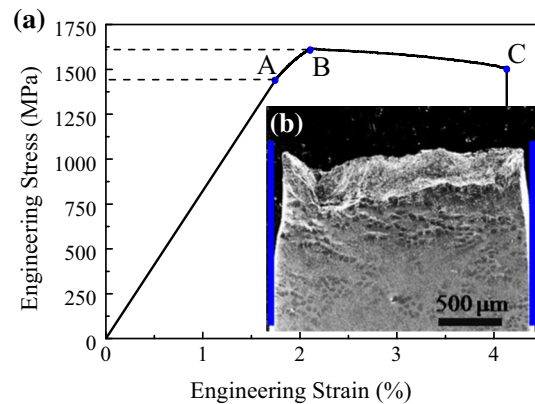


Fig. 2—(a) The uniaxial tensile stress–strain relation of Ti-based MGM composites; (b) The macroscopic fracture with necking behavior.

### B. Tension Properties and Deformation

Figure 2 displays the uniaxial tension stress-strain curve of the composite. The yielding strength and ultimate tensile strength are of 1460 and 1611 MPa, as shown in Figure 2(a). The curve exhibits a linear-elastic response with the elastic modulus of 81.9 GPa, followed by work-hardening and work-softening behaviors. The considerable plasticity of the specimen can be observed by the large plastic strain (Figure 2(a)) and the necking behavior (Figure 2(b)), which is consistent with the previous results.<sup>[3,4,7–10]</sup>

Figure 3 shows the specimen surface SEM images of the tensile fracture. The profuse shear bands and slip bands distributed near the fracture surface, as shown in Figure 3(a). In the glass matrix, the primary shear bands with the spacing of 5 to 10 μm and secondary shear bands with the spacing of 1 to 3 μm extended along different shear plane (Figure 3(b)), which is similar to that of monolithic MGs.<sup>[1,2]</sup> However, in the dendrite phase, numerous slip bands with the spacing of ~200 nm propagated along the different direction resulting in the micro-voids or cavities, as displayed in Figure 3(c). The slip bands banked out when they passed across the fine dendrites, resulting in the profuse shear bands, as shown in Figure 3(d). The shear bands passed through the



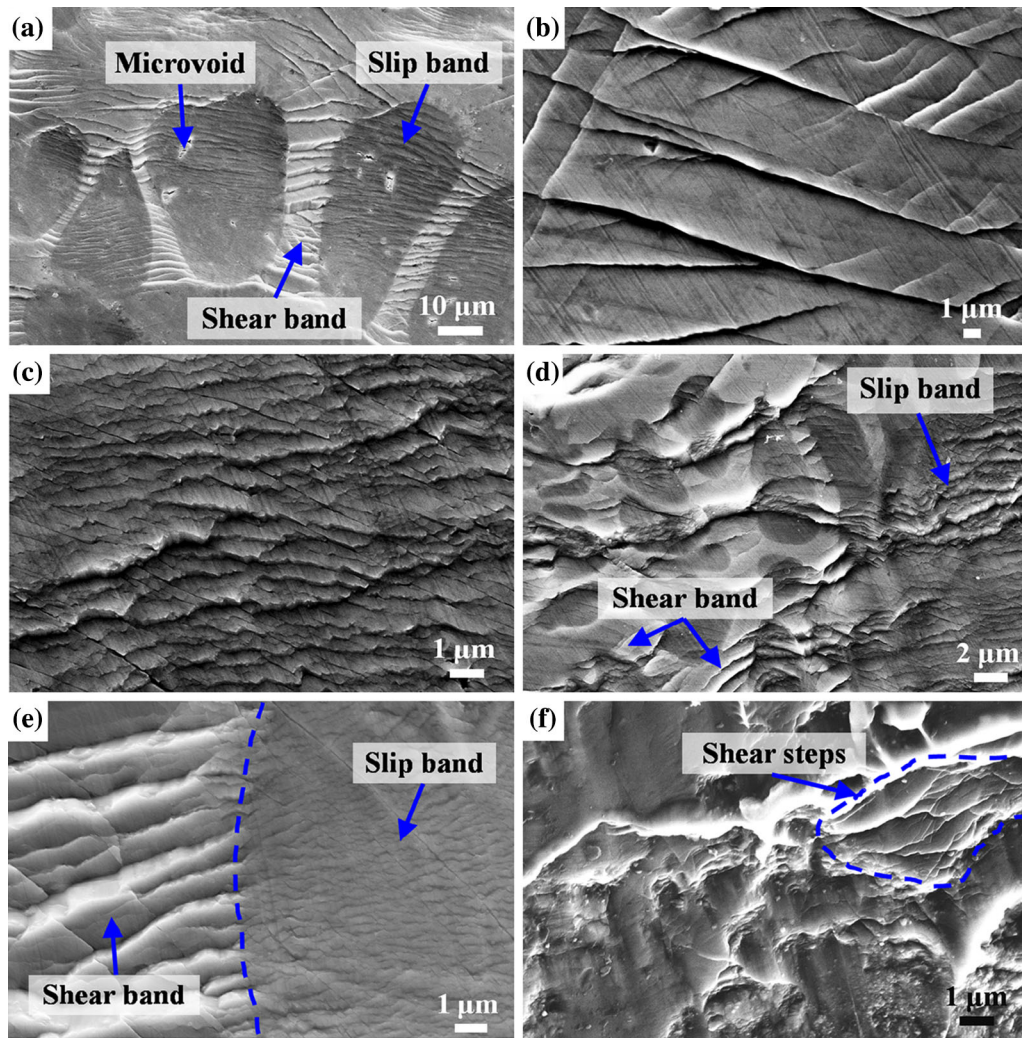


Fig. 3—SEM micrographs of the fracture specimens: (a) the low magnification fractured surface; (b) the fractured feature in the glass phase; (c) the deformation feature in dendrite phase; (d) and (e) the fractured feature nearby the interface; (f) the fractured characteristics.

dendrites by forming many jogs nearby interface, moreover, initiated a great deal of fine slip bands in different directions instead of shear bands, as illustrated in Figure 3(e). It plays a key role in constraining the quick propagation of shear bands, because the formation of these fine slip bands relieves the stress concentration in the neighborhood of interface, leading to the improvement of the plasticity.<sup>[18-21]</sup> Figure 3(f) shows the fracture SEM images of the composite. Clearly, the shear steps formed along difference shear planes which stacked on each others.

The notion that the multiplication of shear bands plays the positive role for the improvement of the plasticity is widely accepted in amorphous materials. An equation was proposed to characteristic the plastic strain,  $\varepsilon^*$ , on the basis of the geometrical observation of shear bands:<sup>[26]</sup>

$$\varepsilon^* = \rho_s \cdot \lambda, \quad [1]$$

where  $\rho_s$  is the shear band density ( $\rho_s = d^{-1}$ ) and  $d$  is the shear band spacing which can be got from

Figure 3(c).  $\lambda$  is the critical shear offset, which is of 0.1 to 0.5  $\mu\text{m}$ . Here, if  $\lambda = 0.2 \mu\text{m}$  and  $d = 8 \mu\text{m}$ , the contribution of the shear bands to the total the plastic strain can be estimated as  $\sim 2.5$  pct, which is consistent with previous result of Zr-based MGM composite.<sup>[3,27]</sup>

### C. Microscopic Deformation Investigation by In Situ TEM Tension

Figure 4(a) displays the micro-crack propagation in the glass matrix. At fracture region, the fracture surface consists of shear steps over several hundred nanometers, as shown in Figure 4(a) and marked by "b" in Figure 4(a). According to the image contrast in Figure 4(b), numerous shear planes stacked on the top of each other instead of an individual shear plane to form shear steps, which is consistent with the case in monolithic BMGs.<sup>[28]</sup> The shear deformation region corresponding to the band-like-thinned deformation zone formed without generating new surface at the tip of the crack, as shown in Figure 4(c), which is considered as "liquid-like layer" for local intense heating.<sup>[18,20]</sup>

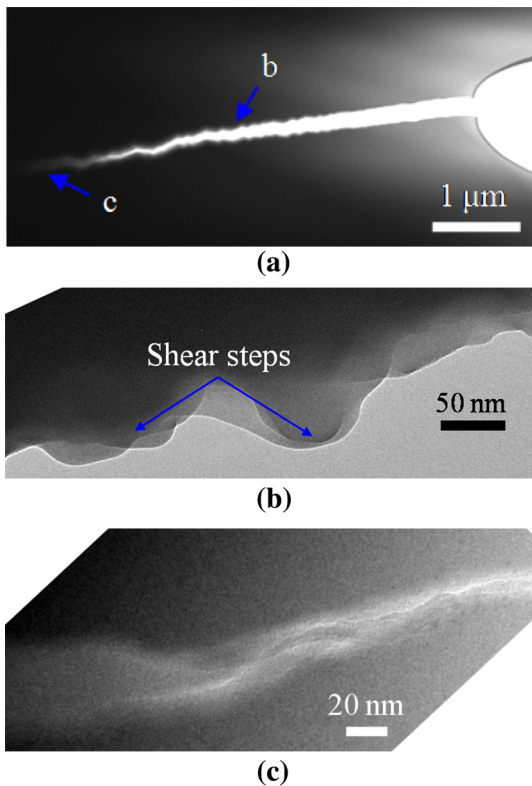


Fig. 4—(a) *In situ* tensile TEM image of the glass matrix fracture characteristic at the low magnification; (b) the fracture feature of localized shear planes stacked on each other, as marked by “b” in (a); (c) the deformation characteristic at the crack tip, as marked by “c” in (a).

Figure 5 shows the shear deformation at micro-crack tip in the glass phase. The band-like-thinned shear deformation zone “AB” is formed ahead of the micro-crack tip along the shear stress direction, where “A” is the tip of the micro-crack, as marked in the image Figure 5(a). It is believed that the narrow shear zone has the lower density and strength than the intact region, which may be condensed into nano-voids for the presence of atomic clusters and the free volume.<sup>[29,30]</sup> As the deformation proceeds, the applied stress increased gradually. Once the applied stress condition satisfied the stress which required propagating the pre-existing shear band, the stress equilibrium ahead of the tip would be destroyed. The pre-existing shear band propagation is impeded to fulfill the stress equilibrium; the generation of the new surface is preferentially by local atomic clusters instead of the nucleation, as shown in Figure 5(b). The shear deformation zone “AB” acts as a guild to lead the rapid propagation during further loading. In the shear deformation zone, the nanocrystallization could be initiated by the releasing of the local heating.<sup>[19,23,25–27,29]</sup> The propagated distance is of ~200 to 500 nm, which is consistent with previous reports in monolithic BMGs.<sup>[20,25]</sup>

The basic fracture features under *in situ* TEM tension of the dendrite is shown in Figure 6(a). In the plastic deformation zone ahead of the crack tip in the dendrite, numerous dislocation walls and profuse dislocations can

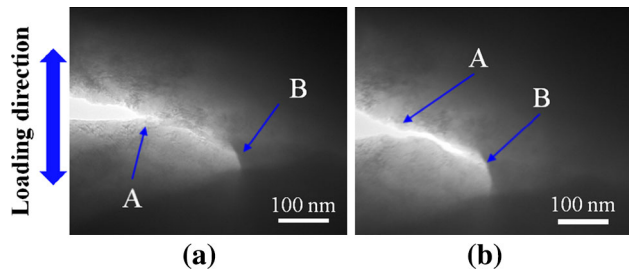


Fig. 5—*In situ* tensile TEM images of shearing event in the amorphous phase: (a) a pre-micro-crack; (b) the propagation of the micro-crack after further loading.

be observed in Figures 6(b) and (c). Micro-void formed at the micro-crack tip, as shown in Figure 6(d). It provided direct evidence that the propagating crack from the glass matrix to the dendrite phase was arrested by the plastic deformation of the dendrite. So, when a micro-crack propagated between the brittle glass matrix and the ductile dendrite phase, as shown in Figure 7(a), the ductile dendrites can prohibit efficiently by its plastic deformation. With the applied stress increasing, the crack quickly passed across the glass phase without retention, but the propagation direction changed, as marked in Figure 7(b). It is related to the coefficient of internal friction, the dilatancy factor, and the stress state.<sup>[31]</sup> Then, the crack was stopped in the other dendrite. However, for monolithic BMGs, the micro-crack can propagate about ~5  $\mu\text{m}$  along the principal stress direction due to absence the propagated resistance.<sup>[20,25]</sup>

#### IV. DISCUSSION

For *in situ* MGM composites, the stress–strain curve can be divided into the elastic stage, the work-hardening stage, and work-softening stage by yielding strength and the ultimate tensile strength, as shown in Figure 2(a). It is result of the competition between the dislocation mechanisms of the dendrite phase and the free volume mechanisms of the glass phase. Here, a model for plastic flow localization was employed to express each deformation stages.<sup>[4,8]</sup>

Initially, both the dendrite and glass phase of *in situ* MGM composites deformed elastically,<sup>[4,8]</sup> as marked by “0A” in Figure 2(a) and as shown in Figure 8(a).

$$\sigma = E\varepsilon \quad 0 \leq \varepsilon < \varepsilon_y, \quad [2]$$

where  $\varepsilon_y$  is the yielding strain. Subsequently, the ductile dendrite yields first by dislocations, but the glass matrix deformed elastically for the nucleation rate of free volume keep a balance with the annihilation rate,<sup>[9,10,29–34]</sup> as shown in Figure 8(b). Here, it can be got on the stress–strain curve as the deviation from linearity strain of 1.64 pct, as marked by “A” in Figure 2(a). When the accumulation of the net free volume reaches at the critical volume content, the glass phase yielded. However, the contribution from work hardening of dendrites is stronger than the softening



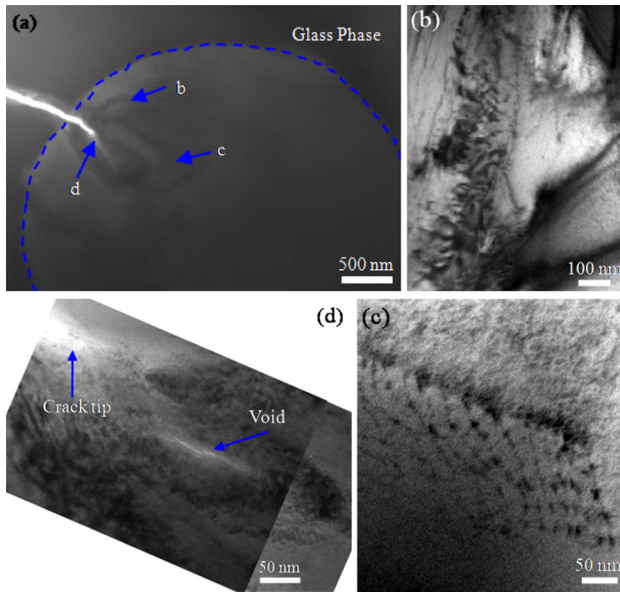


Fig. 6—(a) the low magnification *in situ* tensile TEM image of an arrested propagating crack by the plastic zone in the dendrite; (b) and (c) the plastic deformation caused by dislocations and dislocation wall; (d) the plastic deformation feature ahead of the crack tip.

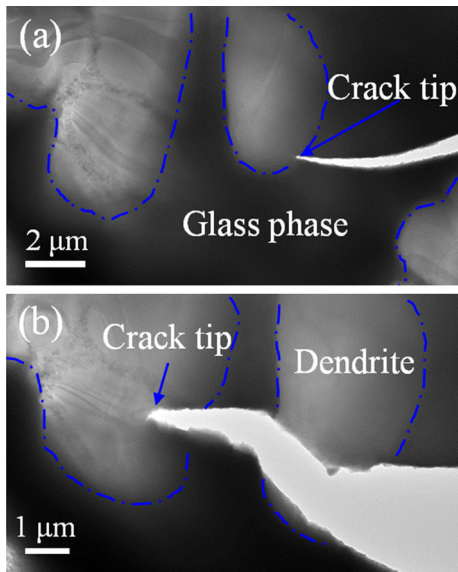


Fig. 7—The expansion process of the micro-crack between the two phases: (a) the crack tip was prohibited by the dendrite; (b) the crack passed across a fine dendrite and the glass phase, but stopped by a coarse dendrites.

effect of the glass matrix at the beginning of the forming shear bands. So, the work-hardening behavior of dendrites is still dominating the deformation,<sup>[9,10]</sup> as marked by “AB” in Figure 2(a). As loading proceeds, the softening effect of glass phase balances the work-hardening effect of dendrites, leading to the ultimate tensile strength, as marked by the point “B” in Figures 2(a) and 8(c). As a result, the stress–strain curve exhibits the work-hardening stage, which can be expressed as:

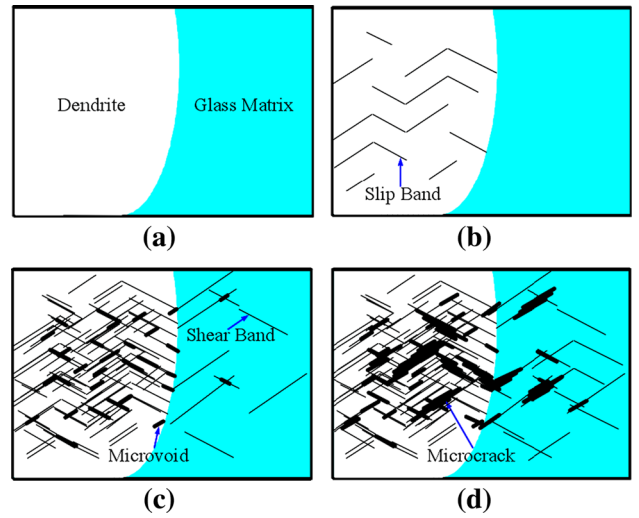


Fig. 8—A schematic diagram of the deformation characteristics of the MGM composites: (a) the elastic stage, both phases underwent the elastic deformation; (b) the yielding stage, the local plastic deformation started in dendrite phase but the glass phase keep the elastic deformation; (c) the work-hardening stage, the glass phase started shear deformation, but the plastic deformation of the dendrite phase dominated the deformation; and (d) the work-softening stage, the shear deformation in the glass matrix dominant the deformation.

$$\sigma = \sigma_y + E_h(\varepsilon - \varepsilon_y) \quad \varepsilon_y \leq \varepsilon < \varepsilon_y + \varepsilon_s, \quad [3]$$

$$\varepsilon_s = \frac{\sigma_y}{E_y} + \frac{\sigma_{uts} - \sigma_y}{E_h}, \quad [4]$$

where  $\sigma_y$ ,  $\sigma_{uts}$ ,  $\sigma_f$ , and  $\varepsilon_t$  are the yielding strength, ultimate tensile strength, fracture strength, and ultimate tensile strain, respectively.  $E_y$  is Young’s modulus, and  $E_h$  is work-hardening modulus. Usually, the strain of the work-hardening stage is very limited for the *in situ* MGM composites reinforced by the  $\beta$ -dendrite phase, such as ~1.0 pct in Ti-based MGM composites.<sup>[9]</sup> Here, the strain of this stage is of ~0.4 pct.

At next deformation stage, the long-range internal stresses induced structural variations and atomic rearrangements near the shear band lead to the reduction of the hardness and modulus. So, the required stress for shear bands propagation is lower than the stress for shear bands nucleation, resulting in the reduction of macro-stress,<sup>[29–34]</sup> as marked by “BC” in Figures 2(a) and 8(d)

$$\sigma = \sigma_{uts} - E_s(\varepsilon - \varepsilon_y - \varepsilon_s) \quad \varepsilon_y + \varepsilon_s \leq \varepsilon, \quad [5]$$

where  $E_s$  is the softening modulus. For the dendrite phase,<sup>[12,13,34]</sup> although the stress continually increased because the sustained localized necking, the resistance to softening dominated by shear banding is evidently decreased, resulting in the softening of the composite. At the work-softening stage, the slip bands or shear bands occur in localized region,<sup>[12,13,35–37]</sup> but the local instable shear deformation can be counterbalanced by the plastic deformation of the dendrite. Therefore, the local deformation can be transferred between the

dendrite and the glass matrix. The considerable macro-plastic deformation is achieved by reproduce this processes. Typically, the plastic flow can occur within the ductile dendrite after voids grow significantly and start to coalesce.<sup>[35–37]</sup> However, the brittle failure can also be triggered immediately by void-nucleation in the glass phase as void-nucleation mode. At the last stage, the plastic deformation of dendrite phase by dislocations cannot offset the quickly extension of shear bands, resulting in the final failure.

## V. CONCLUSIONS

In this investigation, the detailed study on the fracture and deformation of the Ti-based metallic glass matrix composite has been studied by the multidimensional investigation including the tensile test and *in situ* TEM tension test. The tension stress–strain curve of the composite exhibits not only high strength but also the considerable plasticity. Microscopically, it is found that shear deformation zone formed at the crack tip in glass phase, but the plastic deformation was initiated ahead of dendrites. Dendrites can effectively restrict the propagation of the shear band for the excellent plastic deformation ability. The attributions of micro-deformations to the strength and plasticity of composites were discussed.

## ACKNOWLEDGMENTS

Authors are grateful for the financial support of the National Basic Research Program of China (973 Program No. 2011CB605501) and the National Natural Science Foundation of China (Nos. 51001008, 51101110, and 51371122).

## REFERENCES

- J.J. Lewandowski and A.L. Greer: *Nat. Mater.*, 2006, vol. 5, pp. 15–18.
- S.V. Ketov and D.V. Louzguine-Luzgin: *Sci. Rep.*, 2013, vol. 3, pp. 1–6.
- D.C. Hofmann, J. Suh, A. Wiest, G. Duan, M. Lind, M.D. Demetriou, and W.L. Johnson: *Nature*, 2008, vol. 451, pp. 1085–89.
- D.C. Hofmann, J. Suh, A. Wiest, G. Duan, M. Lind, M.D. Demetriou, and W.L. Johnson: *Proc. Natl. Acad. Sci. USA*, 2008, vol. 105, pp. 20136–40.
- S. Pauly, G. Liu, G. Wang, U. Kühn, N. Mattern, and J. Eckert: *Acta Mater.*, 2009, vol. 57, pp. 5445–53.
- Y. Wu, H. Wang, H.H. Wu, Z.Y. Zhang, X.D. Hui, G.L. Chen, D. Ma, X.L. Wang, and Z.P. Lu: *Acta Mater.*, 2011, vol. 59, pp. 2928–36.
- G. Chen, J.L. Cheng, and C.T. Liu: *Intermetallics*, 2012, vol. 28, pp. 2825–33.
- R.L. Narayan, P.S. Singh, D.C. Hofmann, N. Hutchinson, K.M. Flores, and U. Ramamurty: *Acta Mater.*, 2012, vol. 60, pp. 5089–5100.
- J.W. Qiao, A.C. Sun, E.W. Huang, Y. Zhang, P.K. Liaw, and C.P. Chuang: *Acta Mater.*, 2011, vol. 59, pp. 4126–37.
- J.W. Qiao, T. Zhang, F.Q. Yang, P.K. Liaw, S. Pauly, and B.S. Xu: *Sci. Rep.*, 2013, vol. 3, pp. 1–6.
- Y.J. Huang, J.C. Khong, T. Connolly, and J. Mi: *Appl. Phys. Lett.*, 2014, vol. 104, pp. 031912–16.
- F.F. Wu, Z.F. Zhang, and S.X. Mao: *Acta Mater.*, 2009, vol. 57, pp. 257–66.
- F.F. Wu, K.C. Chan, S.S. Jiang, S.H. Chen, and G. Wang: *Sci. Rep.*, 2014, vol. 4, pp. 5302–08.
- J.C. Lee, Y.C. Kim, J.P. Ahn, and H.S. Kim: *Acta Mater.*, 2005, vol. 53, pp. 129–39.
- H.F. Zhou, S.X. Qu, and W. Yang: *Int. J. Plast.*, 2013, vol. 44, pp. 147–60.
- Y.P. Jiang and K. Qiu: *Mater. Des.*, 2015, vol. 65, pp. 410–16.
- H.L. Jia, L.L. Zheng, W.D. Li, N. Li, J.W. Qiao, G.Y. Wang, Y. Ren, P.K. Liaw, and Y.F. Gao: *Metall. Mater. Trans A*, 2015, vol. 46A, pp. 2431–42.
- M. Legros, D.S. Gianola, and K.J. Hemker: *Acta Mater.*, 2008, vol. 56, pp. 3380–93.
- H. Lu, Y. Su, Y. Wang, and W. Chu: *Corros. Sci.*, 1999, vol. 41, pp. 699–708.
- D.T.A. Matthews, V. Ocelík, P.M. Bronsveld, and J.T.M. De Hosson: *Acta Mater.*, 2008, vol. 56, pp. 1762–73.
- G. Wilde and H. Rösner: *Appl. Phys. Lett.*, 2011, vol. 984, pp. 251904–07.
- E. Pekarskaya, C.P. Kim, and A.W.L. Johnson: *Mater. Res Soc.*, 2001, vol. 16, pp. 2513–18.
- Y.S. Wang, Z.X. Guo, R. Ma, G.J. Hao, Y. Zhang, J.P. Lin, and M.L. Sui: *Prog. Nat. Sci.: Mater. Int.*, 2014, vol. 24, pp. 121–27.
- Y.S. Wang, G.J. Hao, Y. Zhang, J.P. Lin, and J.W. Qiao: *Metall. Mater. Trans A*, 2013, vol. 45A, pp. 2357–63.
- J.T.M. De Hosson: *Microsc. Res. Tech.*, 2009, vol. 72, pp. 250–60.
- H. Bei, S. Xie, and E.P. George: *Phys. Rev. Lett.*, 2006, vol. 96, pp. 105503–07.
- C.C. Hays, C.P. Kim, and W.L. Johnson: *Phys. Rev. Lett.*, 2000, vol. 84, pp. 2901–04.
- S.F. Guo, K.C. Chan, Q. Chen, J.J. Li, and L. Liu: *Scripta Mater.*, 2009, vol. 60, pp. 369–72.
- M.Q. Jiang, Z. Ling, J.X. Meng, and L.H. Da: *Philos. Mag.*, 2008, vol. 88, pp. 407–26.
- M. Heggen, F. Spaepen, and M. Feuerbacher: *J. Appl. Phys.*, 2005, vol. 97, pp. 33506–14.
- Y.F. Gao, L. Wang, H. Bei, and T.G. Nieh: *Acta Mater.*, 2011, vol. 59, pp. 4159–67.
- J.F. Knott: *Fundamentals of Fracture Mechanics*, Butterworth, London, 1973.
- L.F. Liu, L.H. Dai, Y.L. Bai, and B.C. Wei: *J Non-Cryst. Solids*, 2005, vol. 351, pp. 3259–70.
- Q. Xue, M.A. Meyers, and V.F. Nesterenko: *Acta Mater.*, 2002, vol. 50, pp. 575–96.
- Y. Shen and G.P. Zheng: *Scripta Mater.*, 2010, vol. 63, pp. 181–84.
- Z. Lu, W. Jiao, W.H. Wang, and H.Y. Bai: *Phys. Rev. Lett.*, 2014, vol. 113, pp. 045501–05.
- F.F. Wu, S.T. Li, G.A. Zhang, X.F. Wu, and P. Lin: *Appl. Phys. Lett.*, 2013, vol. 103, pp. 151910–13.